Tracking and Understanding Dynamics of Atoms and Clusters of Late Transition Metals with *in-situ* DRIFT and XAS Spectroscopy Assisted by DFT

Bidyut Bikash Sarma*[1,2], Jelena Jelic[1,2], Dominik Neukum[1,2], Dmitry E. Doronkin,[1,2] Xiaohui Huang,[3,4], Felix Studt[1,2] and Jan-Dierk Grunwaldt[1,2]

[1]Institute for Chemical Technology and Polymer Chemistry, Karlsruhe Institute of Technology, Engesserstraße 20, 76131 Karlsruhe, Germany

[2]Institute of Catalysis Research and Technology, Karlsruhe Institute of Technology, Hermann-von-Helmholtz Platz 1, 76344 Eggenstein-Leopoldshafen, Karlsruhe, Germany

[3]Institute of Nanotechnology, Karlsruhe Institute of Technology, Hermann-von-Helmholtz Platz 1, 76344, Eggenstein-Leopoldshafen, Karlsruhe, Germany

[4]Department of Materials and Earth Sciences, Technical University Darmstadt, Alarich-Weiss-Str.2, 64287, Darmstadt, Germany

ABSTRACT: Dynamic structural changes of single atom catalysts (SACs) are key to many reactions that were reported to be catalyzed by supported single atoms. To understand these changes, systematic *in-situ* diffuse reflectance infrared spectroscopy (DRIFTS) and X-ray absorption spectroscopy (XAS) experiments were carried out under reducing (1% CO) and oxidizing (1% CO + 1% O_2) reaction atmosphere at room temperature over CeO_2 supported late transition metals (Ru, Rh, Pd, Ir and Pt) synthesized via two different methods (wet impregnation and precipitation) to take into account influence of surface properties. As a general trend, the CO vibrational frequencies downshifted under CO atmosphere which we assigned to formation of clusters. Upon changing the gas mixture to more oxidizing (1% CO + 1% O_2), single sites are retained as evidenced by the CO vibrational frequencies at higher wavenumbers. Among the investigated metals, Pt^{2+} and Pd^{2+} are more prone to cluster formation and Rh^{3+} and Ru^{4+} are found to be stable as single site following the order Rh > Ru > Ir > Pt > Pd. In combination with DFT calculations of the CO vibrational frequencies we are able to assign shifts to changes in oxidation state of the metals. These findings thus serve as a benchmark for ceria supported Pd, Pt, Ru, Ir, Rh SACs.

Keywords: Single atom catalysts, DRIFT spectroscopy, XAS spectroscopy, clusters, DFT calculations

1. INTRODUCTION: A recent blooming area in the field of heterogeneous catalysis is to anchor isolated transition metal atoms over solid support and their application in various catalytic processes such as thermal, electrochemical and photochemical conversions.[1-5] For some of the highly important industrial reactions that were shown to be catalyzed by supported nano-particles (NPs), recent investigations indicate that well-decorated atoms over solid support as the catalytically active centers could outperform NPs in these reactions.[6] Moreover, the tunable charge and coordinating behavior of single atom catalysts (SACs) make them unique and similar to molecular catalysts. Hence through SACs, one can bridge the knowledge between homogenous and heterogeneous catalysis.[7] In this context, it is attractive to understand CO insertion reactions since they play a vital role, both in homogeneous and heterogeneous catalysis. For example, Rh complexes can catalyze hydroformylation in the liquid phase, whereas Rh NPs are active for higher alcohol synthesis, with CO insertion being a common step in both processes.[8] Recent work by various researchers showed that Rh SACs are also active for hydroformylation.[9-10] Similarly, an Ir single atom catalyst was also shown to be effective for carbonylation of methanol to produce acetic acid,[11] which is catalyzed by molecular Ir or Rh complexes on an industrial scale.[12-14] Moreover, Pd is known to catalyze a series of carbonylation reactions in liquid phase.[8, 15] This raises the following questions: (a) can we transfer the knowledge between molecular catalysis and heterogeneous catalysis via the carbonylation reaction as a common platform, (b) whether it is a metal single site that is catalytically active or whether the dynamic structural changes of SACs play an essential role under operating conditions as indicated by many researchers[16-18] and (c) is there any trend in CO binding behavior that directly or indirectly depends on catalyst loading, method of preparation and surface area of the resulting catalysts with metals from different rows in the periodic table? Hence, herein we focus on an in-depth understanding of the dynamics of atoms with *in-situ* X-ray absorption spectroscopy (XAS)[19] and diffuse reflectance infra-red fourier transform (DRIFT) spectroscopy using a series of 4d (Ru, Rh and Pd) and 5d (Ir and Pt) elements under CO and CO + O_2 reaction conditions.

Ceria (CeO_2) has been widely studied for its exceptional properties such as its oxygen storage capacity and ability to stabilize isolated atoms, clusters and nano-particles, making it ideal for many catalytic applications.[20] It is a redox active support and the easy formation of defect sites over ceria can serve as binding locations for isolated noble metals.[21-22] The low index surfaces along (111), (110) and (100) facets are thermodynamically stable with a terminating oxygen layer on top.[23] The coordination number of both Ce and O is lower on the surface than in bulk. Besides, the (111) surface is easily reducible, so defect formation is favorable. Incorporating metals in isolated form can compensate the defect site formation by directly occupying those sites with strong covalent bonds to the CeO_2 support.

Late transition metal-based single atom catalysts have been shown to be active for many reactions where CO is present in the feedstock or product. For example, CO oxidation,[1, 24] water gas shift,[25] reverse water gas shift,[26] hydroformylation,[9-10] the carbonylation of methanol,[11] etc. For CO oxidation reaction that was reported to be catalyzed by Pt single site over $CeO_{2,}$[21] recent operando investigations have shown that Pt clusters are the true active species and the single sites act as spectator.[16] A synergy between metallic and oxidized Pt sites is also possible during CO oxidation by Pt/CeO_2 as observed by Meunier *et al.*[27] This study complements the claims made by Koplent *et al.* where both short lived Ce^{3+} was found as active species during CO oxidation whereas long lived Ce^{3+} species present as inactive spectator.[28] Recently Escobar-Bedia *et al.* claimed Ru single sites to be highly active and regio-selective for hydroformylation of alpha olefin, which lack *in-situ* investigations.[29] Often, it is unclear whether the single atom is the active species or whether it transforms to clusters or nano-particles under the reaction conditions due to dynamic structural changes.[30] The CO insertion mechanism for a reaction such as hydroformylation is well known in molecular catalysis.[31-32] Higher alcohol synthesis[33] which also involves a CO hydrogenation step to a Rh-C bond occurs on Rh nano-particles, and details of the mechanism are more sparse.[34] Chuang *et al.* proposed the presence of Rh^+ as the key for CO insertion to produce higher alcohols.[35] In another example, the carbonylation of methanol to produce acetic acid, the CO insertion step on a molecular Ir catalyst is quite different from that of a Rh catalyst and alters significantly the activity and stability of the catalyst.[12]

In this work, we have synthesized atomically dispersed late transition metals (Ru, Rh, Pd, Ir and Pt) supported over ceria with precipitation and wet impregnation methods followed by calcination at 623 K and 1073 K in static air, respectively. The high temperature treatment is well known to generate single sites over ceria[21] whereas precipitation is one of the most commonly practiced methods in industry for the preparation of solid catalysts.[36] Furthermore, the calcination temperature influences the surface area and formation of the defect sites over ceria which could directly correlate with the uniformity of distribution of isolated atoms over the support.[17] Various spectroscopic techniques were used to investigate the local structure of the synthesized catalysts and *in-situ* DRIFTS and XAS were used to understand the dynamic structural changes. In addition, DFT calculations were used to identify the CO vibrational frequencies and we correlated these values to the corresponding Bader charge and CO binding energies of the SACs.

2. EXPERIMENTAL SECTION

2.1. Materials and Methods:

Metal precursors $Rh(NO_3)_3 \cdot xH_2O$ (Sigma Aldrich, 36% Rh basis), $Ru(NO_3)_x(NO)$ (Alfa Aesar, 31.3% Ru), $Pd(NO_3)_2$ (Alfa Aesar, 99.8%), $Pt(NO_3)_2$ (ChemPUR), $Ce(NO_3)_3 \cdot 6\,H_2O$ (Alfa Aesar, 99.5%), $IrCl_3$ (Sigma Aldrich, 99.8%), $Rh(acac)_3$ (Sigma Aldrich, 97%), $Ru(acac)_3$ (Sigma Aldrich, 97%), $Pt(acac)_2$ (Alfa Aesar, 48% Pt), $Pd(acac)_2$ (Sigma Aldrich 99%),

$Ir(acac)_3$ (Alfa Aesar, 37.5%) were used as received. Potassium hydroxide (KOH) and ethanol were purchased from EMPLURA®. Gas mixtures such as 10% CO/Ar, 20% O_2/Ar, 10% H_2/Ar and pure Ar (99,999%) bottles were purchased from Air Liquide.

2.2 Catalyst synthesis: The ceria support was prepared by calcining cerium nitrate hexahydrate precursor at 623 K (ramp rate 2 K/min) under static air for 5 h. The series of late transition metal (Ru, Rh, Pd, Ir and Pt) catalysts were synthesized over ceria support by wet impregnation (WI) and precipitation (PP) methods. For wet impregnation, acetylacetonate precursors of the metals were first dissolved in acetone and then dispersed over ceria. The solution was sonicated for 5 min and the solution was evaporated to dryness under vacuum (500-400 mbar) in a rotary evaporator over 3 hours. The impregnates were further dried in an oven overnight at 353 K in static air. The solids were ground, mixed with mortar and pestle, and finally calcined at 1073 K under static air. For catalysts synthesized via precipitation method, nitrate and chloride salts of Ce and noble metals were first dissolved in water and the pH value of the solution was increased to 10 by adding 1M KOH solution over a period of 3 hours under continuous stirring. At pH 10, the solutions were further kept stirring for another 30 min to achieve a stable pH. The slurry was then transferred into a closed glass vessel and kept at 353 K for 12 h. The solid fractions were centrifuged and washed with distilled water (3 times) followed by ethanol (3 times). The solid was further dried at 353 K for 12 h and ground to fine powder with mortar and pestle. The solids were then calcined at 623 K under static air.

2.3. Characterization of the catalysts:

2.3.1. *Powder X-ray diffraction (XRD):* X-ray diffraction patterns of the powder catalysts were recorded on a PANalytical X'Pert Pro instrument using a Bragg-Brentano geometry with Cu−Kα radiation (1.54060 Å) and a Ni filter. The catalysts were placed on a Si wafer holder. The diffractograms were recorded from 20° to 80° (2θ) over a period of 8 hours (step size of 0.017°, 0.53 s acquisition time, 5 scans) at room temperature. The obtained reflections were compared to reference data sets available in the Joint Committee of Powder Diffraction Standards (JCPD) database.

2.3.2. *Aberration corrected high-angle annular dark-field scanning-transmission electron microscopy (HAADF-STEM):* HAADF-STEM measurements were performed using a C_s-probe corrected Themis 300 from Thermofischer Scientific operated at 300 kV. Finely ground powder samples were dry-cast on Cu grids (Quantifoil company) coated with a Lacey carbon film. The excess powder was removed with an air gun. Energy dispersive X-ray (EDX) mapping were carried out with Super-X EDX detector.

2.3.3. *X-ray absorption spectroscopy:* X-ray absorption spectra were measured at the Ru K-edge (22.117 keV), Rh K-edge (23.220 keV), Pd K-edge (24.350 keV), Ir L_3-edge (11.215 keV), and Pt L_3-edge (11.564 keV). A Si (311) double crystal monochromator (DCM) was used for Ru K-, Rh K- and Pd K-edges, and a Si (111) DCM was used for Ir L_3- and Pt L_3-edges to scan the incident energy. The Ru K-, Rh K- and Pd K-edge spectra were collected at P65 beamline at the Deutsches Elektronen-Synchrotron (DESY), Hamburg, Germany[37] and Ir L_3 and Pt L_3-edge spectra at BM23 beamline at the European Synchrotron Radiation Facility (ESRF), Grenoble, France and at the CATACT beamline of the Karlsruhe Light Source, Karlsruhe, Germany. The measurements were performed in transmission mode (reference samples were diluted with cellulose) or in fluorescence mode (in a quartz capillary micro reactor[38] without any dilution). The XAS data reduction and fitting were carried out using the Demeter software package.[39] Data treatment (alignment, normalization) has been performed using the Athena code (version 0.9.26). For fitting the experimental data, DFT optimized structures and models based on standard crystallographic data were used for all the metals. The k range up to 12 $Å^{-1}$ and R range between 1-3.5 Å were considered for the fits. S_0^2 was derived from the corresponding metallic foil reference spectra to determine the coordination number. The EXAFS equation[40] used for deriving the free parameters is given by

$$\chi(k) = S_o^2 \sum_i N_i \frac{f_i(k)}{kR_i^2} \; e^{-\frac{2R_i}{\lambda(k)}} \; e^{-2k^2\sigma_i^2} \, sin(2kR_i + \; \delta_i(k))$$

Where S_o^2 is the amplitude reduction factor, N is the degeneracy of the scattering path, f(k) is the scattering function, k is the wavenumber, R is the distance between absorber and scatterer, λ is the mean free path of the photoelectron, σ^2 is the mean square radial displacement, also known as the Debye-Waller factor, δ is the phase shift of the couple absorber/scatterer and i represents a particular number of shell. R-factor that is frequently used while reporting quality of fit; represents goodness of the fit.

For *in-situ* XAS measurements, the sieved catalyst fraction (100-200 μm) was filled in a quartz capillary micro reactor (2 mm outer diameter, 0.02 mm wall thickness). Gas mixtures (1% CO or 1% CO + 1% O_2 balanced with Ar) were fed through the capillary with a flow of 30 mL/min. For temperature programmed reduction experiments, the samples were heated to the required temperature with a gas blower (FMB Oxford GSB-1300 at ESRF and Leister LE mini at DESY). Online analysis of the gas mixtures was carried out qualitatively with a mass spectrometer (Pfeiffer Vacuum OmniStar GSD-320).

2.3.4. *XANES simulation*: The theoretical XANES spectra at different edges were calculated by FEFF 9.6.4 code using multiple-scattering theory.[41] DFT-optimized model structures were based on isolated metal atoms placed on 100, 110 and 111 facets of CeO_2. The amplitude reduction factor, S_0^2 was set to 1 and the core-hole was treated with random phase approximation. The radii for full multiple scattering (FMS) and self-consistent field (SCF) calculations were set as 5 Å. The details of DFT calculations are mentioned in the section 2.3.9.

2.3.5. *In-situ diffuse reflectance infra-red spectroscopy*: *In-situ* DRIFTS investigations were carried out on a VERTEX 70 FTIR spectrometer (Bruker) equipped with an *in-situ* diffuse-reflectance optics and a cell (Harrick Praying Mantis and High Temperature Cell) with a CaF_2

window. A sieve fraction of 100-200 μm of the catalyst was used for the measurements. Catalysts were purged with He or Ar via mass flow controller and heated to 573 K for 1 hour to remove any impurity adsorbates. The spectra were collected in reflectance mode between 1000-4000 cm^{-1} with a spectral resolution of 4 cm^{-1}. The spectra are reported in logarithm log(1/R) or in Kubelka-Munk units by converting with the following formula

$$F(R_\infty) = \frac{(1 - R_\infty)^2}{2R_\infty}$$

where R_∞ stands for reflectance of the sample (measured relative to the sample under Ar as a background scan).

For the background spectra, 200 scans were collected and averaged under Ar flow and for the samples 150 scans were collected per measurement. The measurements were performed continuously over 1 hour. The gas mixture at the outlet of the *in-situ* cell was qualitatively analyzed by an online mass spectrometer (Pfeiffer Vacuum OmniStar GSD-320).

2.3.5. *In-situ reduction*: All the catalysts prepared with the precipitation method followed by calcination at 623 K were reduced *in-situ* under 10% H_2/Ar during a temperature ramp from 298 K to 523 K with a ramp rate of 2 K min^{-1} and a dwell time of 30 min. For XAS measurements, the reduction was carried out in a quartz capillary reactor with a catalyst sieve fraction of 100-200 μm. X-ray absorption near edge structure (XANES) spectra were measured continuously during reduction of all the catalysts. Similarly, the *in-situ* reduction was carried out in the DRIFTS cell prior to the DRIFTS measurements. The samples were reduced first *in-situ* at 523 K (ramp 2 K min^{-1}) under 10% H_2/Ar mixture and then pure Ar was flown for one hour before cooling down to room temperature.

2.3.6. *Raman spectroscopy*: Raman spectra were measured using an inVia Reflex Raman Spectrometer system (Renishaw). The spectrometer is equipped with a HeNe Laser (wavelength

633 nm) and a Leica microscope. For all measurements, a 100× objective was used to illuminate the sample in the powder form. The laser intensity was set to 1% (0.043 mW at the sample). Spectra were recorded averaging three acquisitions with an acquisition time of 120 s each at different spots and taken in a range from 200 to 1000 cm^{-1}. All spectra were averaged and baseline-corrected (Origin 2019, adjacent averaging method, smoothening window size 3 and threshold 0.05).

2.3.7. *Quantification of metal content*: Quantitative analysis of the metal content of the catalysts was performed by ICP-OES measurements (Agilent 720/725-ES instrument). 30-40 mg of the samples were digested in a mixture of sulfuric and nitric acid in a microwave digestion system at 453 K for 45 min.

2.3.8. *N_2-physisorption*: Nitrogen physisorption isotherms were recorded at 77 K using a Rubotherm BELSORP-mini II instrument. The specific surface areas were determined by the Brunauer–Emmett–Teller method. Catalysts were degassed at 423 K for 2 h under vacuum prior to the experiment.

2.3.9. *Computational details*: Density functional theory (DFT) calculations were performed using the Vienna Ab Initio Simulation Package (VASP)[42,43] in connection with the Atomic Simulation Environment (ASE).[44] A plane-wave basis set with a cutoff energy of 450 eV, the projector augmented wave method (PAW)[45,46] and the Bayesian Error Estimation Functional with van der Waals correlations (BEEF-vdW)[47] were used. For better description of localized Ce 4f electrons, the GGA+U method[48] was applied. As described in earlier work, we found a value of U = 5 eV to be reasonable when employing the BEEF-vdW functional.[49] Four layers thick 2x2 large unit cells were used to represent CeO_2 (111) and CeO_2(110) infinite slab models and 4x2 large unit cells were used to represent the CeO_2 (100) surface. All slabs were separated by more than 15 Å of vacuum in the z direction. We investigated all five transition metals M (Ru, Rh, Ir, Pt and Pd) single atoms catalysts with MOx being in the three formal oxidation states M, MO and MO_2. All atoms in the top two layers of the CeO_2 (111), (110) and (100) surface as well as the MO_x single atom clusters were allowed to relax during geometry optimizations. The Brillouin zones were sampled using a (4x4x1) Monkhorst-Pack k-point grid[50] for CeO_2(111) and (110) and a (3x6x1) k-point grid for CeO_2(100). The convergence criterion for geometry optimizations was a maximum force of 0.01 eV/Å. Spin polarization was considered in all calculations.

3. RESULTS

3.1. *Synthesis and characterization of atomically dispersed catalysts*: Catalysts synthesized *via* wet impregnation and precipitation showed a typical metal content in the range of 0.6-0.9 wt% as shown in the electronic supplementary information (ESI), figure S1 (b). The BET surface area analysis showed that wet impregnated catalysts calcined at 1073 K had a lower surface area (30-60 m^2/g) whereas catalysts prepared via precipitation method followed by calcination at 623 K showed relatively high surface area (90-120 m^2/g) as shown in figure S1 (a). The lower surface area of the bare CeO_2 (10 m^2/g) calcined at 1073 K is due to the sintering of the ceria particles at high temperature. Upon addition of metal dopants, ceria gains extra stability against sintering as reported.[16, 22] Importantly, the catalysts prepared via the precipitation method retain their surface area comparable to the bare CeO_2 (101 m^2/g) since the sintering of the CeO_2 particles at low temperature (623 K) is less likely to occur.

The powder XRD patterns showed that the support is highly crystalline after calcination. No reflection from metal crystalline phases (2 Theta~40^0) of Ru, Rh, Pd, Ir and Pt, irrespective of the preparation method were observed confirming that the metals are highly dispersed over the support and lack of long range order as shown in figure S2-S6. The aberration-corrected (C_s) high angle annular dark field (HAADF) scanning transmission electron microscope (STEM) images and the corresponding elemental mapping of the catalysts prepared via precipitation (figure 1) showed that all the metals are in highly dispersed state. In the case of Pt/CeO_2 and

Ir/CeO_2, the z-contrast difference is sufficiently large to observe the single atoms as shown in figure 1 (a) and (b). However, in the case of Ru, Rh and Pd, it is challenging to identify single atoms as shown in figure 1 (c)-(e). Energy dispersive X-ray (EDX) mapping confirms the presence of all these metals uniformly over ceria support as shown in figure S7-S11. The Raman spectra showed the presence of metal-oxygen-cerium vibrational modes in all the catalysts prepared via precipitation method more distinctly than the one prepared via impregnation method as shown in figure S12-S16. This indicates that most of these noble metals in catalysts prepared via the precipitation method are uniformly doped in the ceria lattice. In case of Rh and Ir supported over CeO_2 catalysts showed more O-vacancies (600 cm^{-1}) in comparison to Ru, Pd and Pt. This can be attributed to the mis-match of the valence state of Rh and Ir atoms when they are incorporated in the CeO_2 lattice. The CeO_2 supported Pt, Rh and Ru catalysts prepared via impregnation method and calcined at 1073 K are reported earlier.[22]

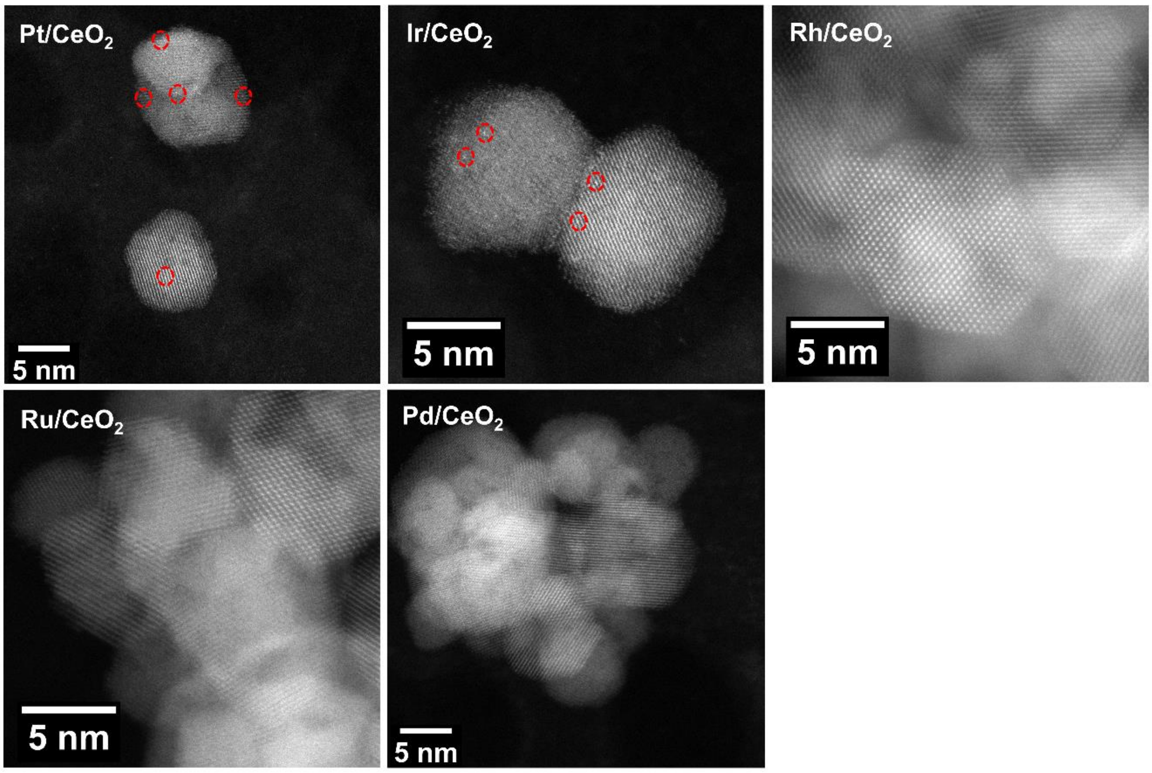

Figure 1. Aberration corrected HAADF-STEM images of Pt, Ir, Rh, Ru and Pd dispersed over CeO_2 via precipitation method (calcined at 623 K). Dotted circles represents the single atom of

Pt and Ir. The corresponding EDX mapping are shown in figure S7-S11 of the ESI. Scale bar in all the images are 5 nm.

X-ray absorption spectroscopy is indispensable[51] in identifying the local geometry of the supported metals prepared by the two different methods. Analysis of the Fourier transformed (FT) extended X-ray absorption fine structure (EXAFS) spectra of all the metals showed presence of M-O as the first shell around 1.5 Å (phase uncorrected) and a minor feature around 3 Å. To derive the coordination numbers and to fit the scattering features in the first and second shells, reference crystallographic data were taken. The experimental data and the fits are shown in figure 2. The free parameters derived from the corresponding fits are listed in table S1. It is evident that the second feature are contributions from the M-O-Ce scattering and not from the presence of any bulk oxide of the corresponding metals, which is along the line of the results obtained from the Raman spectroscopy. We further carried out simulation of XANES spectra using FEFF 9.6.4 code on DFT-optimized model structures of all the metals over 100, 110 and 111 facets of CeO_2 as shown in figure S17-S31. These results show that the 4-fold coordinated isolated metals over the 100 facet resemble closely the experimental spectra. Maurer *et al.* reported that adsorbed Pt^{2+} shows better stability compared to PtO_2 (gas phase) over the CeO_2 (100) facet when calcined at 1073 K.[16] Moreover, above 773 K restructuring of CeO_2 is highly likely.

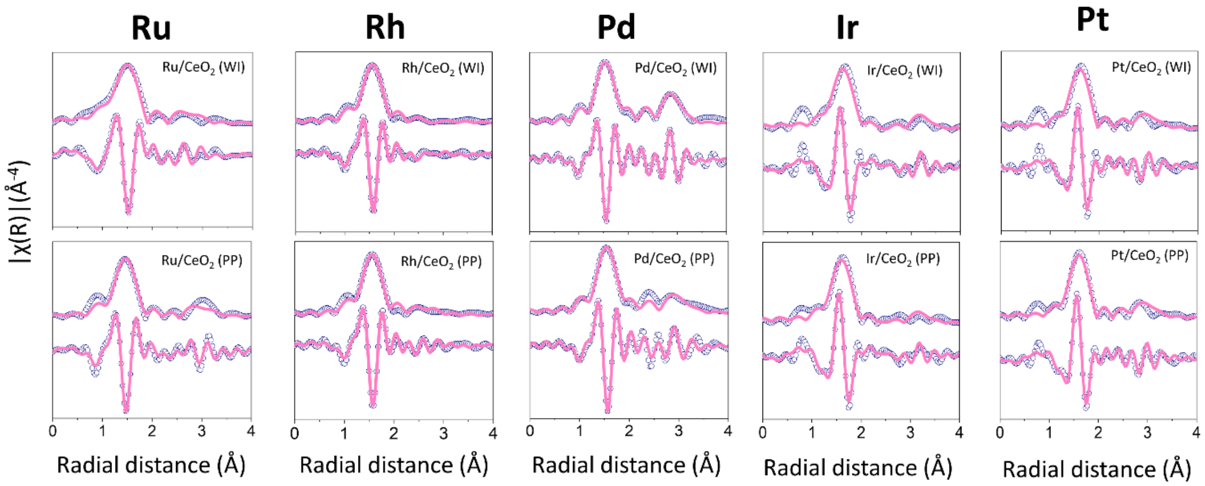

Figure 2. FT k^3-weighted EXAFS spectra (navy, open circle) and fit (pink, solid line) of all metals supported over CeO_2 synthesized via precipitation (PP) and wetness impregnation (WI). Both magnitude (top) and imaginary (bottom) components are shown. Fitting parameters are shown in table S1 of the ESI.

3.2. ***Theoretical XANES spectra and DFT calculated phase diagram***: Theoretical XANES spectra of the DFT optimized structures showed that the spectra of the isolated species of these metals closely resemble the metal over 100 facet of CeO_2 compared to 110 and 111 facets (figure 3). The phase diagrams (bottom, figure 3) of the isolated metals over CeO_2 (100) further suggest that all metals are in their highest formal charge state (M_1O_2) with the exception of Pd. For Pd we found a charge of 2+ (Pd_1O). The DFT-calculated phase diagrams over CeO_2 (111) are shown in figure S32. From the comparisons of the phase diagrams, it is evident that the as synthesized isolated metals distributed over the CeO_2 (100) surface are more stable than the CeO_2 (111) surface alone. Moreover, the stability of the single sites increases with formal oxidation states at lower temperature range (0-400 K). At higher temperature (400-800 K) entropic effects favor formation of lower oxidation states. Among the five metals, RuO_2/CeO_2 (100) showed the highest stability whereas Pd and Pt are least stable.

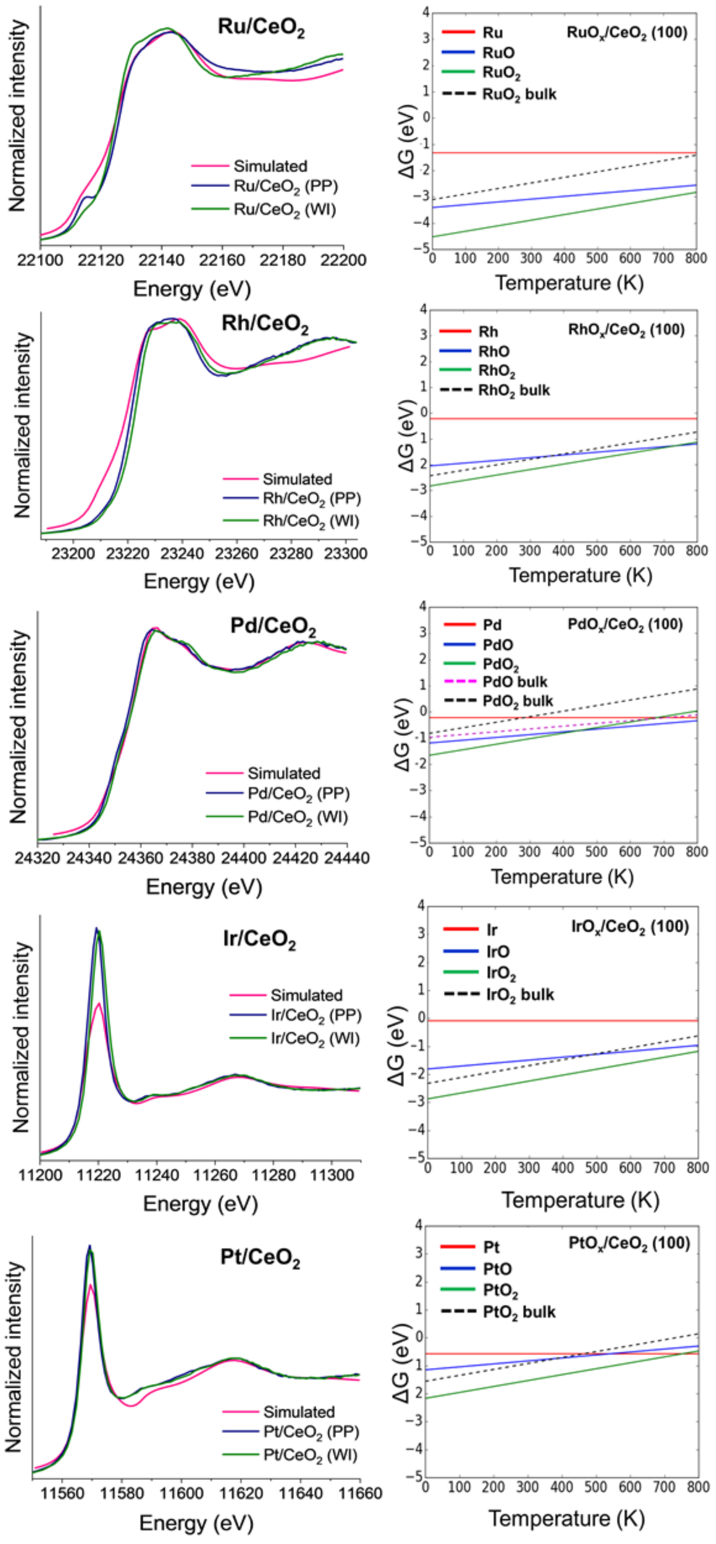

Figure 3. Theoretical XANES spectra (left) obtained from DFT optimized model structures of Ru, Rh, Pd, Ir and Pt and corresponding phase diagrams (right) over the CeO$_2$ (100) facet. The M, MO and MO$_2$ represent isolated metal atoms over CeO$_2$ with different formal oxidation

states. Theoretical XANES spectra of all metals of the DFT-optimized model structures as well as the phase diagrams are shown in figures S17-S32. The ΔG value correspond to 1 bar of O_2.

3.3. *In-situ* XAS and DRIFTS experiments: *In-situ* spectroscopic studies were carried out under CO and CO + O_2 reaction conditions with continuous gas flows to understand CO binding to the catalysts synthesized by wet impregnation and precipitation methods. DRIFTS spectroscopy has been a valuable tool in identifying charged states and coordinating environment of supported isolated metal with probe molecules like CO.[52-54] The late transition metals under consideration here (Ru, Rh, Pd, Ir and Pt) are well known to bind CO. In fact, these metals are the most studied for CO oxidation, which is extremely important for exhaust gas aftertreatment.[55-60] Additionally, these metals are less abundant and to use each and every atom efficiently is crucial. Hence, narrowing down to atomically dispersed species of these metals opens up new possibilities such as CO insertion mechanism which is currently established in molecular catalysis. Since CO is a strong reductant it is quite evident that the local structure of the isolated sites may also change upon its exposure. To understand the dynamics, we carried out a series of *in-situ* XAS and DRIFTS in reducing (1% CO) and oxidizing (1% CO + 1% O_2) environment at room temperature over a time period of one hour. The evolution of different species over time in the DRIFTS spectra is shown in figures 4 and 5. The corresponding *in-situ* XANES and EXAFS spectra collected before and after (1 hour) exposure to the reaction mixtures are represented in figures S33-S37. From the DRIFTS spectra of the catalysts prepared via precipitation it is noticeable that under CO environment the atomically dispersed metals form a series of species at low wavenumbers. After the gas mixture is changed to CO + O_2, new species were formed. In order to predict the origin of these CO vibrational frequencies over these metals, DFT calculations served as a comparison and are shown on the right hand side of figure 4.

3.3.1. *Catalysts synthesized via precipitation (PP)*: (A) Ru/CeO_2: The DRIFTS spectra in Figure 4 (a) and (b) showed a structural change of the Ru/CeO_2 catalyst when exposed to 1% CO and 1% (CO + O_2) gas mixtures. The CO vibrational frequencies at 1982 cm^{-1} (which developed over time) and at 2053 cm^{-1} (blue-shifted from 2042 cm^{-1}) can be assigned to symmetric and asymmetric vibrations of CO bound to ruthenium atom as also observed in the literature.[61] DFT calculation of the CO vibrational frequency also showed two peaks at 1971 cm^{-1} and 2049 cm^{-1} that could be assigned to the geminal dicarbonyl species as shown in figure 4 (c). The observed CO vibrational frequency at 2120 cm^{-1} can be assigned to a Ru single site over CeO_2 as the DFT calculated value indicated a CO vibration around 2106 cm^{-1}. Li *et al.* suggested that this peak can originate from multiple CO adsorbed over a positively charged Ru site.[62] When the gas composition is changed from CO to CO+O_2, the ratio of these peaks changes. The intensity of the peak at 2120 cm^{-1} substantially increases compared to the CO only atmosphere. The peaks at the lower wavenumbers (1920-1950 cm^{-1}) is not observed anymore. This infers that the composition of the gas mixture plays a significant role in maintaining a particular state (charge and coordination) of the Ru single sites. The CO vibrational frequency at 2173 cm^{-1} is attributed to weakly bound CO over the CeO_2 support[63-65] or gas phase CO as this peak disappears after flushing with Ar. We could confirm this by measuring the CO adsorption over bare CeO_2 as discussed below. *In-situ* XAS spectra at the Ru K-edge also show that the intensity of the white line decreases under reducing atmosphere (figure S33) meaning Ru is getting reduced. In contrast, under CO + O_2 environment, there is hardly any change in the white line intensity as shown in figure S33 (a) and (b). The XANES region of the as-synthesized catalyst also shows a pre-edge peak[66] which confirms the presence of non-centrosymmetric Ru in 4 or 5-fold coordination. Upon exposure to CO or CO + O_2, the pre-edge peak disappears due to the change in the local environment of the Ru isolated site. EXAFS spectra before and after the exposure of gas mixtures show changes in the Ru-O first shell which is slightly shifted to the right. Additionally, a new feature appeared between 2.2-2.3 Å which is due to the Ru-Ru scattering as shown in figure S33 (e) and (f), confirming that the local environment around the Ru sites has changed due to cluster formation.

(B) Rh/CeO_2: Upon exposure to CO, the Rh catalyst showed mainly two CO vibrational peaks at 2000-2020 cm^{-1} and 2070-2090 cm^{-1} as shown in figure 4 (d). These peaks correspond to the asymmetric and symmetric stretching vibrational frequencies of linearly adsorbed geminal dicarbonyls over a Rh single site, respectively.[67-69] These results are corroborated by the DFT calculations shown in figure 4 (f). When CO + O_2 gas mixtures were introduced a new shoulder feature appeared around 2114 cm^{-1} (figure 4 (e)) which can be ascribed to CO adsorbed on 4-fold coordinated Rh as RhO_2 according to the DFT investigation (2109 cm^{-1} in figure 4 (f)). Hülsey *et al.* assigned this peak to CO adsorbed over Rh^{3+} species.[58] DFT calculations showed that this peak also matches with CO adsorbed over bulk RhO_2. However, the XANES and EXAFS spectra at room temperature did not show any significant change in the edge and the white line features or presence of any Rh-O-Rh scattering as shown in figure S34 (a), (b), (e) and (f). This means that with a constant supply of oxygen, Rh isolated sites maintain a certain charge and coordination state and are highly stable under these environments, making Rh SACs suitable for studies like CO insertion and CO hydrogenation reactions.

(C) Pd/CeO_2: The supported Pd isolated sites showed a drastic change when exposed to CO as indicated by the CO vibrational frequencies at low wavenumbers in the range of 1950-2070 cm^{-1} shown in figure 4 (g). We assign the peak at 2061 cm^{-1} to CO linearly bound over Pd surfaces and at 1985 cm^{-1} to bridged CO as assigned by DFT calculations. Jbir *et al.* assigned the peak below 2000 cm^{-1} to bridged CO and between 2050-2080 cm^{-1} to CO linearly adsorbed over Pd clusters.[70] When the gas mixture was switched from CO to CO + O_2, a new series of peaks appeared in the range of 2100-2150 cm^{-1} (figure 4 (h)) that can be assigned to CO vibrational frequencies associated with CO bonded over isolated Pd sites as shown in figure 4 (i). DFT calculations suggest that the CO vibrational frequencies at 2105 and 2136 cm^{-1} are associated with Pd single sites over CeO_2. Muravev *et al.* also observed a similar CO vibrational peak with Pd catalysts prepared via flame spray pyrolysis.[59] The Pd K-edge XANES spectra showed a decrease in white line intensity upon exposure to CO (figure S34 (a) and (b)) confirming that Pd is reduced. The EXAFS spectra also showed a clear indication of the presence of Pd-Pd scattering for the sample exposed to CO (figure S34 (e)). Presence of a small fraction of Pd clusters for CO + O_2 atmosphere cannot be neglected as the EXAFS spectra demonstrate a weak Pd-Pd scattering feature in figure S34 (f).

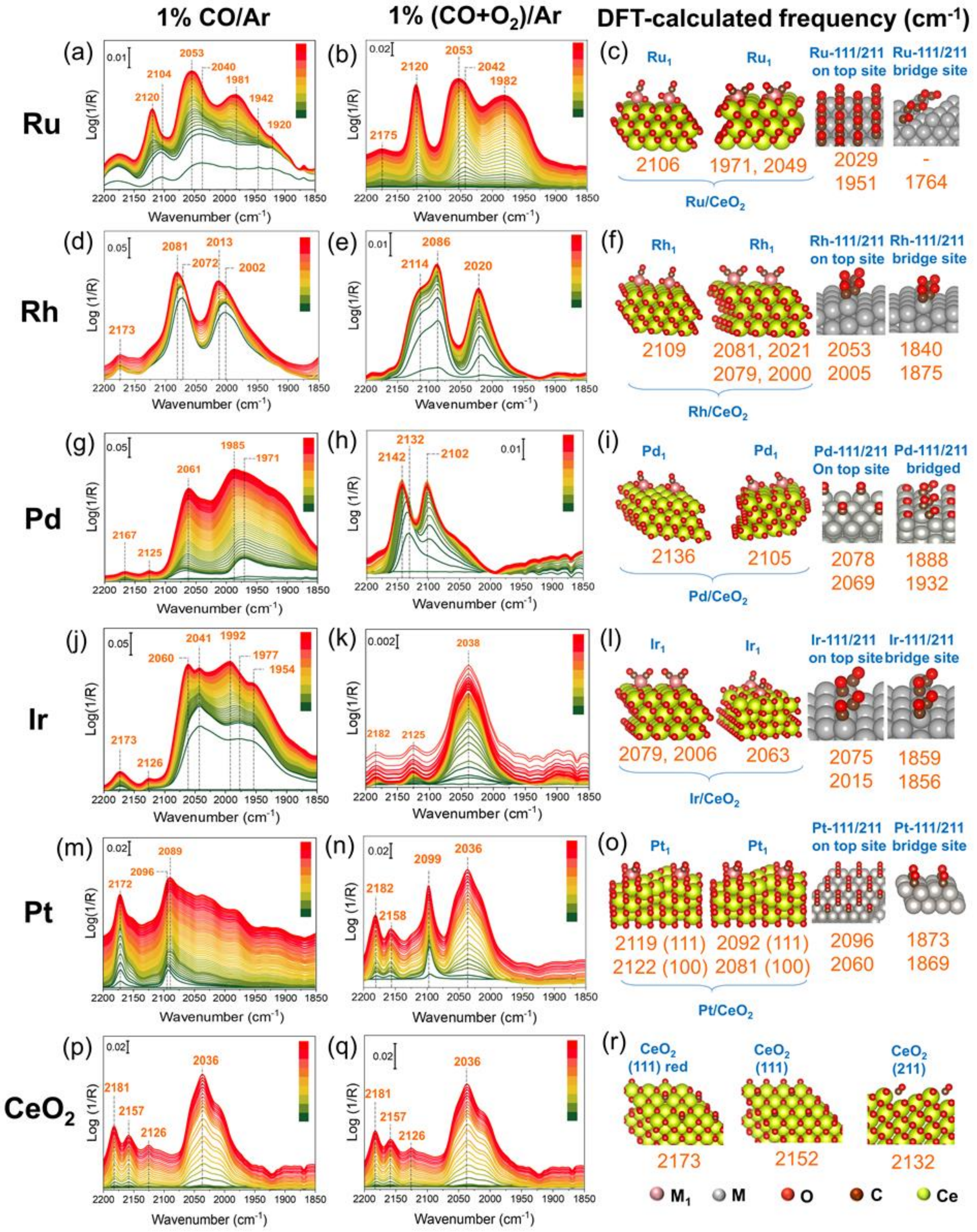

Figure 4. DRIFTS spectra (left and middle column) of CO adsorption at room temperature over catalysts prepared by precipitation method (calcined at 623 K) and DFT calculated CO vibrational frequencies together with the optimized structures (right column). The DRIFTS

spectra were collected with a flow of 1% CO and 1% CO + 1% O_2 over 1 hour. (a)-(c) Ru/CeO_2, (d)-(f) Rh/CeO_2, (g)-(i) Pd/CeO_2, (j)-(l) Ir/CeO_2, (m)-(o) Pt/CeO_2 and (p)-(r) CeO_2. For pure metal, the DFT-calculated CO adsorption frequencies over 111 and 211 facets are shown for a coverage of 0.5 monolayer. The color bar in the figure represents spectra collected over 1 hour.

(D) Ir/CeO_2: Ir samples upon exposure to CO showed two distinct CO vibrational bands at 2041 and 1954 cm^{-1} (figure 4 (j)) which can be attributed to symmetric and asymmetric CO vibrational modes of $Ir(CO)_2$ according to literature.[71-72] Over the time two other CO vibrational frequencies could be observed at 1992 and 2060 cm^{-1}. DFT calculations, however suggest that dicarbonyl vibrations over Ir single sites are at 2006 and 2079 cm^{-1} and that a monocarbonyl vibration is at 2063 cm^{-1} as shown in figure 4 (i). According to DFT calculations, the CO adsorbed over pure Iridium shows CO vibrational frequencies at 2075 cm^{-1} and 1916 cm^{-1} which are assigned to linear and bridged carbonyl. After switching the gas mixture to CO + O_2, no peak related to a CO vibrational frequency over Iridium was observed. This means the Ir sites in the presence of O_2 are somehow blocked and CO cannot reach these sites or the binding interaction of CO is too weak. The XANES and EXAFS spectra at the Ir L_3-edge did not show any detectable changes in the oxidation state and local structures of Ir before and after purging with the CO and CO + O_2 gas mixture as shown in figure S36 (a), (b), (e), and (f) respectively.

(E) Pt_1/CeO_2: The Pt samples on exposure to CO showed a series of peaks in the range of 1900-2090 cm^{-1} that can be assigned primarily to CO vibrational frequencies related to linearly bonded CO over Pt clusters as shown in figure 4 (m). When changing the gas mixture from CO to CO + O_2 (figure 4 (n)), a major peak at 2099 cm^{-1} appears that can be assigned to CO bounded to a Pt isolated site on the CeO_2 (111), (110) or (100) facet. Kottwitz *et al.* have recently elucidated the local structure of atomically dispersed Pt over CeO_2 and assigned the CO vibrational frequency at 2090 cm^{-1} to CO adsorbed atop $Pt^{\delta+}$ or Pt^0.[73] A similar observation was also made by Aleksandrov *et al.,*[74] Maurer *et al.*,[16] and Lu *et al.*[75] concluding that the CO vibrational frequency at 2095 cm^{-1} is from single site Pt species. A separate study by Resasco *et al.* claimed that the CO vibrational frequency between 2090-2100 cm^{-1} could be assigned only to CO adsorbed over a small PtO_x cluster.[17] The authors claims are based on experiments performed over low loaded Pt (0.05 wt%) catalyst that did not show any CO adsorption. Only at a Pt loading of 1 wt% they observed a pronounced CO vibrational frequency at 2096 cm^{-1}. However, for a low loading of 0.05 wt% it cannot be neglected that Pt can occupy sub-surface positions as indicated by very high coordination numbers (0.2 wt% Pt/CeO_2).[22] Moreover, in this article,[22] the authors reported that for a loading of 0.2 wt% Rh, there was no CO vibrational band observed at low temperature confirming the fact that with such a low coverage Rh sites are inaccessible to CO. One can thus speculate that Pt can show a similar behavior. The other question is whether it is a special type of isolated Pt that can form only upon calcination at high temperature (above 873 K). However, we do observe a similar peak with the catalysts prepared via the precipitation method (calcined at 623 K). Our DFT calculations suggest that indeed a 4-fold coordinated Pt single site bearing highly positive charge over CeO_2 shows a CO vibrational peak around 2119-2125 cm^{-1} as shown in figure 4 (o). In contrast, Pt single site over CeO_2 bearing low positive charge might appear between 2080-2095 cm^{-1}. This poses the question on whether this could be due to the formation of small PtO_x clusters. The *in-situ* EXAFS spectra at the Pt L_3-edge, however, did not show any presence of PtO_2 species (Pt-O-Pt scattering, figure S37) before and after purging with the CO or CO+O_2 gas mixtures. DFT calculations also suggest that CO linearly bounded to pure Pt (111) surfaces appears at 2096 cm^{-1}. We conclude that Pt/CeO_2 presents a very complex system requiring further investigations. The CO band at 2038 cm^{-1} might be related to impurities as reported by Meunier *et al.*[76] To consider the influence of the Pt coverage on the CO adsorption, we prepared various coverages (1, 10 and 20 atom %) of Pt over CeO_2 via the precipitation method. The DRIFTS spectra recorded during one hour exposure of the catalyst to the CO+O_2 mixture are shown in figure S38 (a)-(c). The XANES and EXFAS spectra of the as-synthesized catalysts are also shown in figure S38 (d)-

(e). The decrease in the white line intensity upon increase in Pt coverage and presence of Pt-Pt scattering suggests that at higher coverages formation of Pt clusters occurs. Nevertheless, the CO absorption frequency shifts to higher wavenumbers (2099 cm^{-1}) only at the low coverage suggesting that at low coverage most Pt atoms are present as positively charged single sites. The XANES spectra at the Pt L_3-edge did not show any significant changes along the white line due to the low sensitivity towards such small changes as shown in figure S37 (a) and (b). A more sensitive technique in this case will be high energy resolution fluorescence detected (HERFD) X-ray absorption near edge spectra (XANES) which was also recently reported by our group.[16]

(F) CeO_2: The CeO_2 support prepared via precipitation showed CO vibrational frequencies at 2181, 2157 and 2126 cm^{-1} (figure 4(p) and (q)). These could be weakly bound CO over the support as also reported by Christopher and co-workers[17] and these peaks immediately disappear upon flushing with Ar. Mudiyanselage *et al.* assigned the peak at 2162 cm^{-1} to CO adsorbed over Ce^{3+}.[77] Binet *et al.* claimed that the CO absorption frequency in the range of 2151-2168 cm^{-1} is due to CO adsorbed on Ce^{4+} cations with different unsaturated coordination.[78] Our DFT investigations found that CO adsorbed over CeO_2 does indeed have prominent peaks at 2173, 2152 and 2132 cm^{-1} over reduced CeO_2 (111), CeO_2 (111) and CeO_2 (211) respectively as shown in figure 4 (r). A prominent peak at lower wavenumbers 2036 cm^{-1} could be assigned to impurities as also reported in the literature on an Au/SiO_2 catalyst.[76, 79-80] In the DRIFTS spectra measured over an inert CaF_2 reference two very weak CO vibrational frequencies at 2172 and 2116 cm^{-1} were observed as shown in figure S39 (b). Our DFT calculations of CO vibrational frequency of $Ni(CO)_4$ adsorbed over CeO_2 (111) facet reveals that the most intense IR peak at 2035.1 cm^{-1} (figure S39(c)). A more detailed experimental investigation is currently underway.

3.3.2. ***Catalysts synthesized via wet impregnation method:*** The DRIFTS spectra of the catalysts prepared via the wet impregnation method showed a similar behavior under oxidizing and reducing environments to those prepared via precipitation. The Ru/CeO_2 catalyst showed multiple bands as shown in figure 5 (a) and (b) at both high and low wavenumbers under reducing environment which means that CO induces significant structural changes in the Ru catalyst. Upon exposure to the CO + O_2 gas mixture the ratio of the peaks changes confirming that the presence of oxygen considerably influences the local environment of Ru species. The CO vibrational band at 2012 cm^{-1}, which was not observed in the catalyst prepared via the precipitation method can be assigned to CO adsorbed over isolated Ru as also suggested by DFT calculations (figure 4(c)). The CO vibrational frequency around 2181 cm^{-1} can be assigned to weakly bound CO on CeO_2 or gas-phase CO as it was also observed for the CeO_2 support alone as shown in figure 5 (k) and (l). In the case of Rh/CeO_2, under the CO + O_2 environment, the 4-fold coordinated Rh single site is observed (corresponding to a CO vibrational band at 2107 cm^{-1}, (figure 5 (c) and (d)) which disappears under reducing condition (only 1% CO). For Pd/CeO_2, the Pd isolated site remains in the isolated form under oxidizing atmosphere (CO + O_2), whereas under reducing environment (CO) it immediately forms clusters and/or particles (figure 5 (e) and (f)). The CO vibrational frequency at 1958 cm^{-1} corresponds to CO bound to Pd (111 or 211) surfaces in a bridged fashion.[81] The Pt/CeO_2 catalyst showed multiple CO bands in the range between 1950-2090 cm^{-1} mainly corresponding to CO adsorbed over Pt clusters in reducing atmosphere (figure 5 (i) and (j)). Upon introducing CO + O_2 gas mixture to to the catalyst, a dominant peak around 2099 cm^{-1} is observed, corresponding to CO linearly adsorbed over the isolated Pt site. For the Ir/CeO_2 catalyst under CO atmosphere, the CO vibrational frequency at 2070 cm^{-1} (figure 5 (g)) can be assigned to IrO isolated species over the CeO2 (111) facet and the peak at 2001 cm^{-1} corresponds to multiple CO adsorbed over the Ir (111) facet. A peak at 1906 cm^{-1} is a bridged CO bonded to Ir clusters. Upon exposure to CO+O_2, a new set of peaks appears in the range of 2035-2050 cm^{-1} (figure 5 (h)) which can be assigned to IrO isolated species over the CeO_2 (100) as found by DFT calculations. The XANES and EXAFS spectra (figure S33-S37) of these catalysts before and after exposure to the reaction mixture correlate with the changes found by the CO-DRIFTS studies. It is traditional that the CO-DRIFTS spectra are usually represented in the Kubelka-Munk (K-M) units rather than absorbance (logarithmic) units. However, it has been discussed in the literature[76] that weak bands cannot be properly represented in K-M units. The differences can be seen by comparing the spectra in logarithmic scale (figure 4 and 5) and in K-M units (figure S41 and S42).

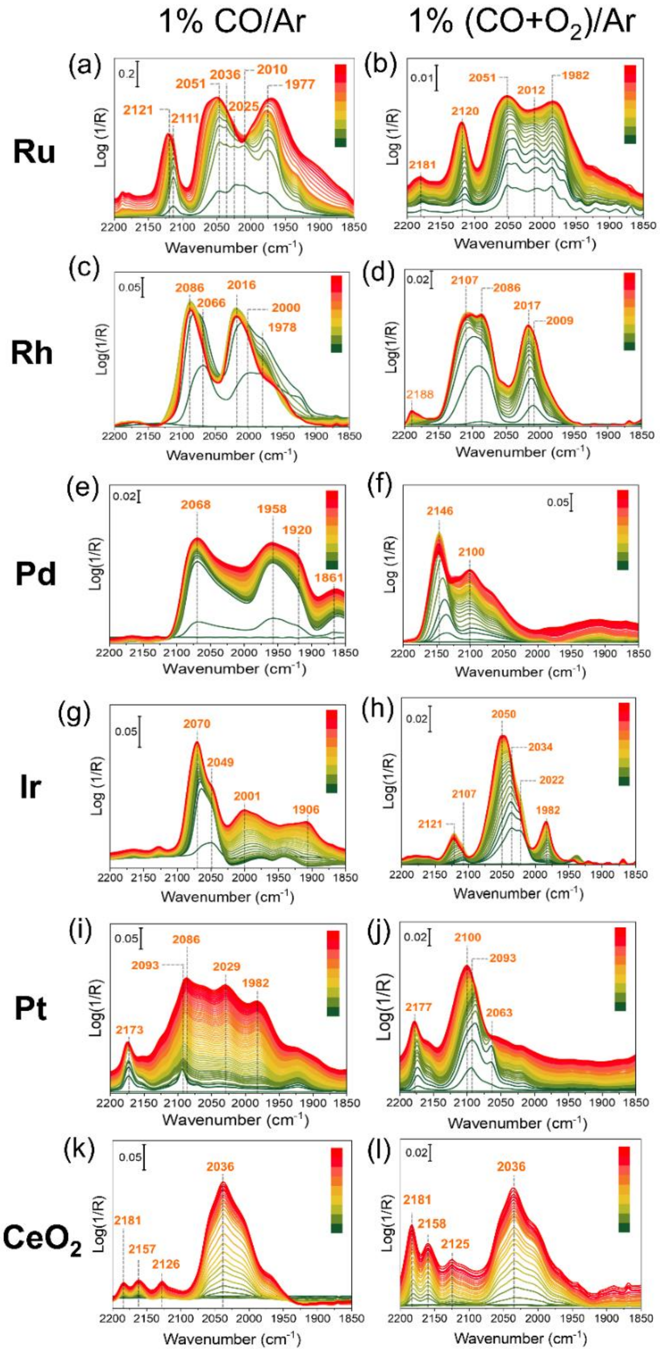

Figure 5. DRIFTS spectra of CO adsorption at room temperature over catalysts prepared by impregnation method (calcined at 1073K). The spectra were collected with a flow of 1% CO and 1% CO +1% O_2) over 1 hour. (a) and (b) Ru/CeO_2, (c) and (d) Rh/CeO_2, (e) and (f) Pd/CeO_2, (g) and (h) Ir/CeO_2, (i) and (j) Pt/CeO_2. The color bar in the figure represents spectra collected over 1 hour.

From the comparison of the DRIFTS spectra of the catalysts synthesized via two different methods, it is evident that irrespective of the preparation method, the SACs showed common features in the presence of CO and CO + O_2 except for Ir/CeO_2. The method of preparation strongly influences the local structure of Iridium atoms and hence CO adsorption over the Ir single atoms. Pd/CeO_2 and Pt/CeO_2 upon exposure to CO immediately formed clusters whereas Rh and Ru SACs are stable under the CO environment over a period of 1 hour. The XANES spectra measured before and after continuous exposure of the gas mixture showed that there are changes along the white line features in case of Ru and Pd. However, in case of Pt and Ir these changes are minor, a more sensitive technique is thus required to follow those changes.

3.3.3. Behavior of *in-situ* reduced catalysts: All catalysts were reduced *in-situ* with 10% H_2/Ar mixture during heating from room temperature to 523 K. The XANES spectra of the temperature-programmed reduction of all catalysts and the corresponding CO DRIFTS spectra are shown in figures S42-S46. In all cases, from the XANES spectra it is evident that there are different degrees of reduction observed for the metals and this reduction should be sufficient to induce cluster and/or particle formation. The more stable the single sites (Ru, Rh and Ir) supported over CeO_2 are, the more difficult it is to reduce them. The DRIFTS spectra of all catalysts showed CO vibrational bands at lower wavenumbers that could be assigned to bridged or linearly bounded CO over metal clusters or nano-particles. In the case of Ru/CeO_2, the CO vibrational frequency at 1967 cm^{-1} is due to CO adsorbed over Ru clusters.[82] It is also clear from the XANES in figure S38 (a) that at 523 K Ru has not been fully reduced as the white line intensity differs from that of Ru foil. For Rh/CeO_2, the CO vibrational frequency at 2057 cm^{-1} could be assigned to CO bound linearly to surface Rh atoms in Rh nano-particles.[83] DFT calculation suggests a peak around 2020 cm^{-1} for the pure Rh metal which is also observed experimentally as shown in figure S39. The Pd/CeO_2 catalyst shows a CO vibrational band between 2000-2060 cm^{-1} which can be assigned to CO bound to Pd clusters as discussed in the previous sections (figure S40 (a)). For Ir/CeO_2, the CO vibrational frequency at 2039 cm^{-1} (figure S41 (b)) can be assigned to CO adsorbed over reduced Ir.[84] The other CO vibrational band at 1978 cm^{-1} can be assigned to CO adsorbed over the Ir(110) surface as indicated by DFT calculations. For the Pt/CeO_2 catalyst, the CO vibrational frequency between 2000-2095 cm^{-1} can be assigned to CO adsorbed on Pt clusters or nano-particles as also reported in literature[85] and found by our DFT calculations and experiments (figure S42 (b)).

3.3.4. Trends in CO binding energy versus Bader charge on the metal: The CO binding energies over different supported single atoms are calculated by DFT. Plots of Bader charges, CO absorption frequency and CO binding energies of single atoms supported over CeO_2 (100) and CeO_2 (111) is shown in the figure 6. These values are also listed in table S2 of the supporting information. The corresponding CO adsorption frequencies are given next to the Bader charge. In general a trend has been observed for the supported isolated metals; with increase in Bader charge the CO binding energy decreases and CO adsorption frequencies increase irrespective of the CeO_2 facet. A deviation to this trend is observed in case of Ru/CeO_2 (111) where the CO binding energy is nearly zero. This might be related to the strong interaction of Ru with the CeO_2 support as it is also difficult to reduce as observed in the temperature programmed XANES spectra at the Ru K-edge (figure S42 (a)). Bulk metals exhibit the highest Bader charge and their CO adsorption frequency is the lowest. At the same time for bulk metal oxides it is the opposite, they exhibit the lowest Bader charge with the highest CO adsorption frequency. The CO binding energy and the adsorption frequencies can change with coverage of CO over the pure metal surface as shown in figure S47. A plot of CO vibrational frequency (cm^{-1}) as a function of a Bader charge (difference of a Bader charge of a metal in a bulk state and supported on CeO_2 surface) for all the single atom at different formal oxidation states is shown in figure S48.

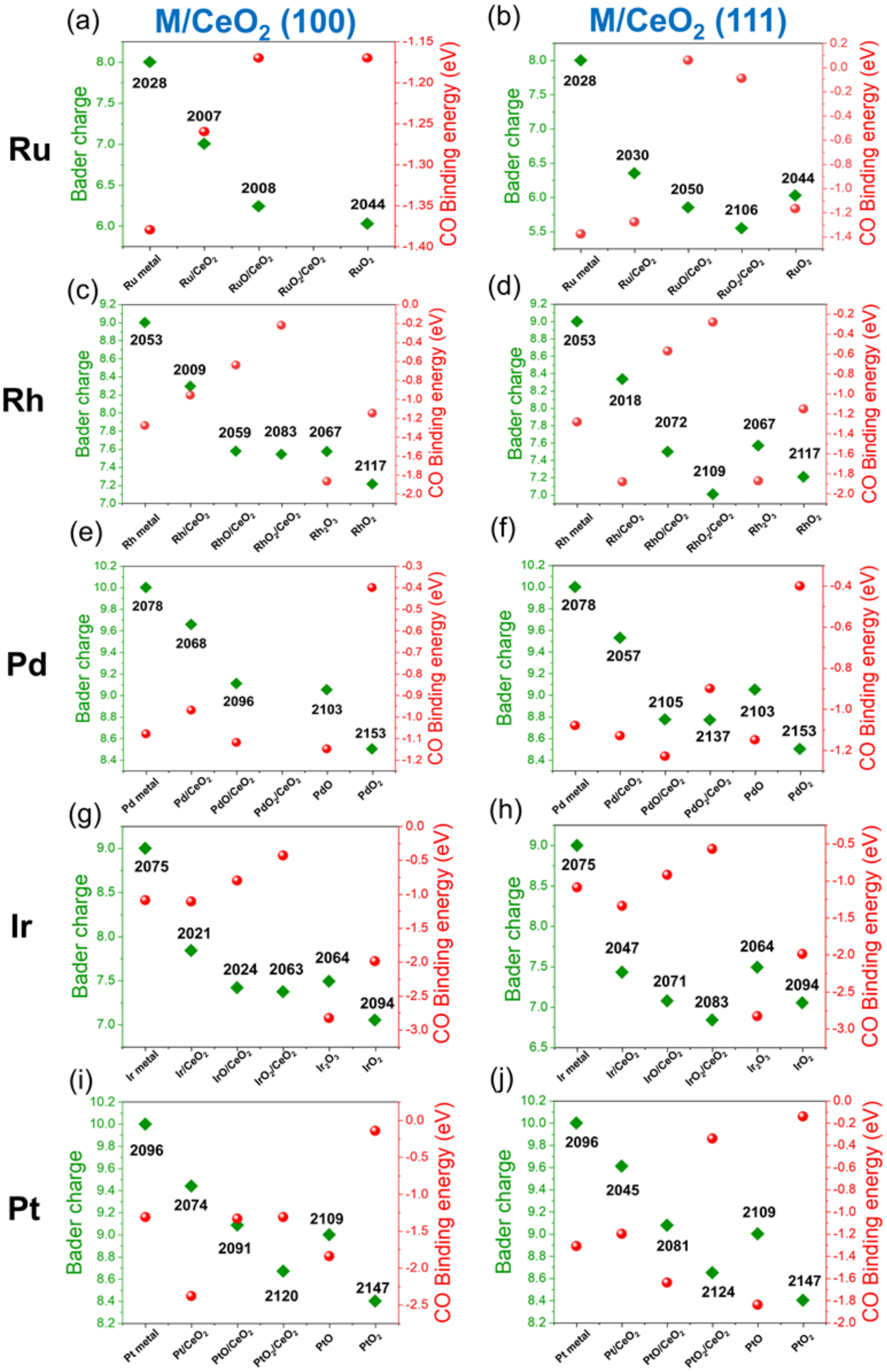

Figure 6. The Bader charge (green square), CO binding energy (red sphere) and the value of CO absorption frequency (cm^{-1}) on single atom supported over CeO$_2$ (100) on the left and CeO$_2$ (111) on the right together with the bulk metal and metal oxides. The Bader charge of the pure metals was considered as the highest. M, MO and MO$_2$ over CeO$_2$ represents supported single atoms.

4. DICSCUSSIONS

In order to investigate the stability of two series of differently synthesized SACs containing noble metals (Ru, Rh, Pd, Ir and Pt) at room temperature, we have performed a series of *in-situ* DRIFTS and XAS experiments under reducing and oxidizing atmospheres. Both DRIFTS and XAS are complementary to each other and we have noticed that in the case of 5d metals (Ir, Pt), changes in the standard XANES regions were not so obvious while DRIFTS showed clear changes in CO vibrational frequencies. The reason for this is that XAS is a bulk technique and small changes might get averaged out; in particular when the single atom sites are very heterogeneous in nature. For all SACs we have observed that CO induces structural changes already at room temperature such that small metal clusters are formed. For the 4d transition metals, Ru and Rh single atoms are less prone to undergo agglomeration whereas Pd and Pt immediately forms clusters especially when the system has been prepared by wet impregnation. When the gas mixture was changed from CO to CO + O_2, all SACs are in oxidized form and the CO vibrational frequencies were shifted to higher wavenumbers as CO is strongly bound to the single atom due to the lack of π back donation from the metal to CO; less availability of electron in the anti-bonding orbital of CO. This trend is observed for all SACs irrespective of the method of synthesis. This highlights the dynamic nature of SACs and shows how different species can evolve over time depending on the reaction condition. The CO induced structural changes can also influence CO adsorption over the SACs and the charge transfer between the support and the single atom can change as shown by Hulva *et al.*[86] Therefore it is necessary to study CO adsorption over time to identify the evolving species.

CO insertion is highly important reaction and can only be investigated in detail through SACs (for solid catalysts) as they closely resemble molecular catalysts. Based on our current study, we further envision to investigate these system with *in-situ*/*operando* DRIFT and XAS spectroscopy in the future. A schematic diagram of stability of various single atom supported over CeO_2 and future possibilities for catalyst design is shown in scheme 1.

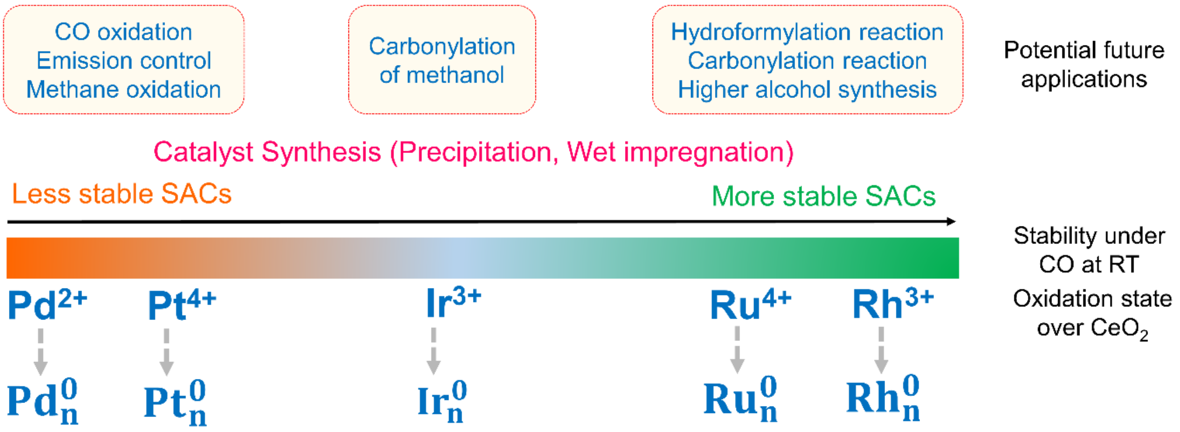

Scheme 1. A schematic of the stability of single atoms supported over CeO_2 with their oxidation state and application for potential reaction is shown.

SACs, a frequently investigated topic in the last decade, various routes have been reported to synthesize them even in large scales. From characterization point of view, high resolution TEM, XAS, low temperature CO FTIR are standard techniques that are used to prove the nuclearity. However, more complementary techniques such as Raman spectroscopy and DFT assisted simulation are necessary since most of the techniques have certain limitations.[87] Moreover, we propose the use of *in-situ* DRIFT spectroscopy as important tool in comparison to conventional XAS to identify such active centers. In the context of those SACs often being used under CO (O_2/H_2) conditions (e.g. Pd and Pt for CO oxidation, Rh for hydroformylation), our study serves as an important benchmark to identify the dynamics of these SACs for these reactions under *in-situ* conditions, in particular the correlation of vibrational shifts with the charge state of the SAC will give important insight into the local surface structure, thus helping to establish structure-activity relationships in future studies.

5. CONCLUSIONS

In conclusion, we have demonstrated the systematic synthesis of SACs of late 5 transition metals (Ru, Rh, Pd, Ir and Pt) via two different preparation methods and characterized the as-synthesized catalysts with N_2-physisorption, C_s-STEM, XRD, Raman, XAS and DRIFT spectroscopy. DFT calculations helped to identify the single sites and the calculated phase diagram showed the preferred locations of the SACs with different formal charges over CeO_2 (100) and (111) surfaces in a temperature range upto 800 K. Among the various metals, Ru and Rh single atoms showed higher stability over CeO_2 and we observed in the temperature-programmed reduction XANES experiments. Moreover, a trend of Bader charge versus the CO binding energy of the supported atoms is observed which showed that CO binding strength increases with decrease in Bader charge of the isolated metal. The calculated XANES spectra showed that the isolated metals bind more strongly to the CeO_2 (100) surface compared to CeO_2 (111). *In-situ* DRIFT and XANES/EXAFS spectroscopy have been successfully applied and tracked the evolution of the isolated metal center over time. Herein we showed that, being a surface sensitive method, DRIFT spectroscopy is an elegant method to probe and follow the structural evolution of SACs. DFT calculations further assisted identifying the various modes of CO adsorption. We believe that this study will serve as a benchmark for the identification and correlation of SACs using CO adsorption as probe reaction.

ASSOCIATED CONTENT

Two separate electronic supporting information files are provided for experimental as well as theoretical work and a file containing all DFT coordinates of the model structures.

AUTHOR INFORMATION

Bidyut Bikash Sarma- Institute for Chemical Technology and Polymer Chemistry, Karlsruhe Institute of Technology, Engesserstraße 20, 76131 Karlsruhe, Germany; Institute of Catalysis Research and Technology, Karlsruhe Institute of Technology, Hermann-von-Helmholtz Platz 1, 76344 Eggenstein-Leopoldshafen, Karlsruhe, Germany, http://orcid.org/0000-0002-5292-7890

Jelena Jelic- Institute for Chemical Technology and Polymer Chemistry, Karlsruhe Institute of Technology, Engesserstraße 20, 76131 Karlsruhe, Germany; Institute of Catalysis Research and Technology, Karlsruhe Institute of Technology, Hermann-von-Helmholtz Platz 1, 76344 Eggenstein-Leopoldshafen, Karlsruhe, Germany.

Dominik Neukum- Institute for Chemical Technology and Polymer Chemistry, Karlsruhe Institute of Technology, Engesserstraße 20, 76131 Karlsruhe, Germany; Institute of Catalysis Research and Technology, Karlsruhe Institute of Technology, Hermann-von-Helmholtz Platz 1, 76344 Eggenstein-Leopoldshafen, Karlsruhe, Germany, https://orcid.org/0000-0002-6013-804X

Dmitry E. Doronkin- Institute for Chemical Technology and Polymer Chemistry, Karlsruhe Institute of Technology, Engesserstraße 20, 76131 Karlsruhe, Germany; Institute of Catalysis Research and Technology, Karlsruhe Institute of Technology, Hermann-von-Helmholtz Platz 1, 76344 Eggenstein-Leopoldshafen, Karlsruhe, Germany, https://orcid.org/0000-0003-3930-3204

Xiaohui Huang- Institute of Nanotechnology, Karlsruhe Institute of Technology, Hermann-von-Helmholtz Platz 1, 76344, Eggenstein-Leopoldshafen, Karlsruhe, Germany; Department of Materials and Earth Sciences, Alarich-Weiss-Str.2, 64287, Technical University Darmstadt, 64289, Darmstadt, Germany.

Felix Studt- Institute for Chemical Technology and Polymer Chemistry, Karlsruhe Institute of Technology, Engesserstraße 20, 76131 Karlsruhe, Germany; Institute of Catalysis Research and Technology, Karlsruhe Institute of Technology, Hermann-von-Helmholtz Platz 1, 76344 Eggenstein-Leopoldshafen, Karlsruhe, Germany, https://orcid.org/0000-0001-6841-4232

Jan-Dierk Grunwaldt- Institute for Chemical Technology and Polymer Chemistry, Karlsruhe Institute of Technology, Engesserstraße 20, 76131 Karlsruhe, Germany; Institute of Catalysis Research and Technology, Karlsruhe Institute of Technology, Hermann-von-Helmholtz Platz 1, 76344 Eggenstein-Leopoldshafen, Karlsruhe, Germany, https://orcid.org/0000-0003-3606-0956

Corresponding Author

Bidyut Bikash Sarma- Email: bidyut.sarma@kit.edu; Phone: +49-(0)721-608-23388

Author Contributions

The manuscript was written through contributions of all authors. All authors have given approval to the final version of the manuscript.

Notes

The authors declare no competing financial interest.

ACKNOWLEDGMENTS

The authors would like to thank Armin Lautenbach for help with ICP-OES analysis, Dr. Sumeet Kale for nitrogen physisorption measurements and Dr. Florian Maurer from KIT for valuable suggestions. We acknowledge KIT Light Source (Karlsruhe, Germany), DESY (Hamburg, Germany), a member of the Helmholtz Association HGF, for the provision of beamtime, allocated to the proposal I-20200891 and ESRF (Grenoble, France) allocated to proposal CH-6119. We would like to thank Dr. Edmund Welter (P65, DESY), Dr. Cesare Atzori (BM23, ESRF) and Dr. Anna Zimina (CATACT, KARA) for assistance in setting up the beamline. HAADF-STEM images and EDX imaging were carried out with the support of the Karlsruhe Nano Micro Facility (KNMFi, **www.knmf.kit.edu**), a Helmholtz Research Infrastructure at Karlsruhe Institute of Technology (KIT, **www.kit.edu**). BBS thank the KIT for the funding of the project. The authors acknowledge support by the state of Baden-Württemberg bwHPC (bwunicluster and JUSTUS, RV bw17D011). JDG and FS further thank Deutsche Forschungsgemeinschaft (DFG, German Research Foundation)-SFB 1441-Project-ID 426888090 (project B3 and B4). Financial support from the Helmholtz Association is also gratefully acknowledged. X. Huang acknowledges the China Scholarship Council (CSC) for PhD programme.

REFERENCES

1. Qiao, B.; Wang, A.; Yang, X.; Allard, L. F.; Jiang, Z.; Cui, Y.; Liu, J.; Li, J.; Zhang, T., Single-Atom Catalysis of CO Oxidation Using Pt_1/FeOx. *Nat. Chem.* **2011**, *3,* 634-641.
2. Wang, A.; Li, J.; Zhang, T., Heterogeneous Single-Atom Catalysis. *Nat. Rev. Chem.* **2018**, *2*, 65-81.
3. Flytzani-Stephanopoulos, M.; Gates, B. C., Atomically Dispersed Supported Metal Catalysts. *Annu. Rev. Chem. Biomol. Eng.* **2012**, *3,* 545-74.
4. Chen, Y.; Ji, S.; Chen, C.; Peng, Q.; Wang, D.; Li, Y., Single-Atom Catalysts: Synthetic Strategies and Electrochemical Applications. *Joule* **2018**, *2*, 1242-1264.
5. Lee, B.-H., et al., Reversible and Cooperative Photoactivation of Single-Atom Cu/Tio2 Photocatalysts. *Nat. Mater.* **2019**, *18*, 620-626.
6. Yang, X.-F.; Wang, A.; Qiao, B.; Li, J.; Liu, J.; Zhang, T., Single-Atom Catalysts: A New Frontier in Heterogeneous Catalysis. *Acc. Chem. Res.* **2013**, *46*, 1740-1748.
7. Cui, X.; Li, W.; Ryabchuk, P.; Junge, K.; Beller, M., Bridging Homogeneous and Heterogeneous Catalysis by Heterogeneous Single-Metal-Site Catalysts. *Nat. Catal.* **2018**, *1*, 385-397.
8. Peng, J.-B.; Geng, H.-Q.; Wu, X.-F., The Chemistry of CO: Carbonylation. *Chem-Us* **2019**, *5*, 526-552.

9. Lang, R., Li, T.; Matsumura, D.; Miao, S.; Ren, Y.; Cui, Y-T; Tan, Y.; Qiao, B.; Li, L.; Wang, A.; *et al.*, Hydroformylation of Olefins by a Rhodium Single-Atom Catalyst with Activity Comparable to RhCl(PPh$_3$)$_3$. *Angew. Chem. Int. Ed.* **2016**, *55*, 16054-16058.
10. Amsler, J.; Sarma, B. B.; Agostini, G.; Prieto, G.; Plessow, P. N.; Studt, F., Prospects of Heterogeneous Hydroformylation with Supported Single Atom Catalysts. *J. Am. Chem. Soc.* **2020**, *142*, 5087-5096.
11. Feng, S.; Song, X.; Ren, Z.; Ding, Y., La-Stabilized, Single-Atom Ir/Ac Catalyst for Heterogeneous Methanol Carbonylation to Methyl Acetate. *Ind. Eng. Chem. Res.* **2019**, *58*, 4755-4763.
12. Haynes, A., Maitlis, P. M.; Morris, G. E.; Sunley, G. J.; Adams, H.; Badger, P. W.; Bowers, C. M.; Cook, D. B.;Elliott, P. I. P.; Ghaffar, T.; et al., Promotion of Iridium-Catalyzed Methanol Carbonylation: Mechanistic Studies of the Cativa Process. *J. Am. Chem. Soc.* **2004**, *126*, 2847-2861.
13. Sunley, G. J.; Watson, D. J., High Productivity Methanol Carbonylation Catalysis Using Iridium: The Cativa™ Process for the Manufacture of Acetic Acid. *Catal. Today* **2000**, *58*, 293-307.
14. Thomas, C. M.; Süss-Fink, G., Ligand Effects in the Rhodium-Catalyzed Carbonylation of Methanol. *Coord. Chem. Rev.* **2003**, *243*, 125-142.
15. Brennführer, A.; Neumann, H.; Beller, M., Palladium-Catalyzed Carbonylation Reactions of Aryl Halides and Related Compounds. *Angew. Chem. Int. Ed.* **2009**, *48*, 4114-4133.
16. Maurer, F.; Jelic, J.; Wang, J.; Gänzler, A.; Dolcet, P.; Wöll, C.; Wang, Y.; Studt, F.; Casapu, M.; Grunwaldt, J.-D., Tracking the Formation, Fate and Consequence for Catalytic Activity of Pt Single Sites on CeO$_2$. *Nat. Catal.* **2020**, *3*, 824-833.
17. Resasco, J., DeRita, L.; Dai, S.; Chada, J. P.; Xu, M.; Yan, X.; Finzel, J.; Hanukovich, S.; Hoffman, A. S.; Graham, G. W.; *et al.*, Uniformity Is Key in Defining Structure–Function Relationships for Atomically Dispersed Metal Catalysts: The Case of Pt/CeO$_2$. *J. Am. Chem. Soc.* **2020**, *142*, 169-184.
18. Liu, L.; Meira, D. M.; Arenal, R.; Concepcion, P.; Puga, A. V.; Corma, A., Determination of the Evolution of Heterogeneous Single Metal Atoms and Nanoclusters under Reaction Conditions: Which Are the Working Catalytic Sites? *ACS Catal.* **2019**, *9*, 10626-10639.
19. Sarma, B. B.; Maurer, F.; Doronkin, D. E.; Grunwaldt, J.-D., Design of Single-Atom Catalysts and Tracking Their Fate Using Operando and Advanced X-Ray Spectroscopic Tools. *Chem. Rev.* **2022**.
20. Montini, T.; Melchionna, M.; Monai, M.; Fornasiero, P., Fundamentals and Catalytic Applications of CeO$_2$-Based Materials. *Chem. Rev.* **2016**, *116*, 5987-6041.
21. Jones, J., Xiong, H.; Delariva, A. T.; Peterson E. J.; Pham, H.; Challa, S. R.; Qi, G.; Oh, S.; Wiebenga, M. H.; Hernandez, X. I. P.; *et al.*, Thermally Stable Single-Atom Platinum-on-Ceria Catalysts Via Atom Trapping. *Science* **2016**, *353*, 150.
22. Sarma, B. B., Kim, J.; Amsler, J.; Agostini, G.; Weidenthaler, C.; Pfänder, N.; Arenal, R.; Concepción, P.; Plessow, P.; Studt, F.; *et al.*, One-Pot Cooperation of Single-Atom Rh and Ru Solid Catalysts for a Selective Tandem Olefin Isomerization-Hydrosilylation Process. *Angew. Chem. Int. Ed.* **2020**, *59*, 5806-5815.
23. Paier, J.; Penschke, C.; Sauer, J., Oxygen Defects and Surface Chemistry of Ceria: Quantum Chemical Studies Compared to Experiment. *Chem. Rev.* **2013**, *113*, 3949-3985.
24. Peterson, E. J., DeLaRiva, A. T.; Lin, S.; Johnson, R. S.; Guo, H.; Miller, J. T.; Kwak, J. H.; Peden, C. H. F.; Kiefer, B.; Allard, L. F.; et al., Low-Temperature Carbon Monoxide Oxidation Catalysed by Regenerable Atomically Dispersed Palladium on Alumina. *Nat. Commun.* **2014**, *5*, 4885.
25. Lin, J.; Wang, A.; Qiao, B.; Liu, X.; Yang, X.; Wang, X.; Liang, J.; Li, J.; Liu, J.; Zhang, T., Remarkable Performance of Ir$_1$/FeO$_x$ Single-Atom Catalyst in Water Gas Shift Reaction. *J. Am. Chem. Soc.* **2013**, *135*, 15314-15317.

26. Aitbekova, A.; Wu, L.; Wrasman, C. J.; Boubnov, A.; Hoffman, A. S.; Goodman, E. D.; Bare, S. R.; Cargnello, M., Low-Temperature Restructuring of CeO_2-Supported Ru Nanoparticles Determines Selectivity in CO_2 Catalytic Reduction. *J. Am. Chem. Soc.* **2018**, *140*, 13736-13745.
27. Meunier, F. C.; Cardenas, L.; Kaper, H.; Šmíd, B.; Vorokhta, M.; Grosjean, R.; Aubert, D.; Dembélé, K.; Lunkenbein, T., Synergy between Metallic and Oxidized Pt Sites Unravelled During Room Temperature CO Oxidation on Pt/Ceria. *Angew. Chem. Int. Ed.* **2021**, *60*, 3799-3805.
28. Kopelent, R.; van Bokhoven, J. A.; Szlachetko, J.; Edebeli, J.; Paun, C.; Nachtegaal, M.; Safonova, O. V., Catalytically Active and Spectator Ce^{3+} in Ceria-Supported Metal Catalysts. *Angew. Chem. Int. Ed.* **2015**, *54*, 8728-8731.
29. Escobar-Bedia, F. J.; Lopez-Haro, M.; Calvino, J. J.; Martin-Diaconescu, V.; Simonelli, L.; Perez-Dieste, V.; Sabater, M. J.; Concepción, P.; Corma, A., Active and Regioselective Ru Single-Site Heterogeneous Catalysts for Alpha-Olefin Hydroformylation. *ACS Catal.* **2022**, *12*, 4182-4193.
30. Gänzler, A. M.; Casapu, M.; Vernoux, P.; Loridant, S.; Cadete Santos Aires, F. J.; Epicier, T.; Betz, B.; Hoyer, R.; Grunwaldt, J.-D., Tuning the Structure of Platinum Particles on Ceria in Situ for Enhancing the Catalytic Performance of Exhaust Gas Catalysts. *Angew. Chem. Int. Ed.* **2017**, *56*, 13078-13082.
31. Sparta, M.; Børve, K. J.; Jensen, V. R., Activity of Rhodium-Catalyzed Hydroformylation: Added Insight and Predictions from Theory. *J. Am. Chem. Soc.* **2007**, *129*, 8487-8499.
32. Imler, G. H.; Zdilla, M. J.; Wayland, B. B., Equilibrium Thermodynamics to Form a Rhodium Formyl Complex from Reactions of CO and H_2: Metal σ Donor Activation of CO. *J. Am. Chem. Soc.* **2014**, *136*, 5856-5859.
33. Luk, H. T.; Mondelli, C.; Ferré, D. C.; Stewart, J. A.; Pérez-Ramírez, J., Status and Prospects in Higher Alcohols Synthesis from Syngas. *Chem. Soc. Rev.* **2017**, *46*, 1358-1426.
34. Choi, Y.; Liu, P., Mechanism of Ethanol Synthesis from Syngas on Rh(111). *J. Am. Chem. Soc.* **2009**, *131*, 13054-13061.
35. Chuang, S. S. C.; Stevens, R. W.; Khatri, R., Mechanism of C2+ Oxygenate Synthesis on Rh Catalysts. *Top. Catal.* **2005**, *32*, 225-232.
36. Ertl, G.; Knözinger, H.; Weitkamp, J.; Preparation of Solid Catalysts. Wiley-VCH, **2008**.
37. Welter, E.; Chernikov, R.; Herrmann, M.; Nemausat, R., A Beamline for Bulk Sample X-Ray Absorption Spectroscopy at the High Brilliance Storage Ring Petra Iii. *AIP Confer. Proc.* **2019**, *2054*, 040002.
38. Grunwaldt, J. D.; Caravati, M.; Hannemann, S.; Baiker, A., X-Ray Absorption Spectroscopy under Reaction Conditions: Suitability of Different Reaction Cells for Combined Catalyst Characterization and Time-Resolved Studies. *Phys. Chem. Chem. Phys.* **2004**, *6*, 3037-3047.
39. Ravel, B.; Newville, M., Athena, Artemis, Hephaestus: Data Analysis for X-Ray Absorption Spectroscopy Using Ifeffit. *J. Syn. Rad.* **2005**, *12*, 537-41.
40. Calvin, S., Xafs for Everyone. *CRC Press Taylor & Francis Group* **2013**.
41. Rehr, J. J.; Albers, R. C., Theoretical Approaches to X-Ray Absorption Fine Structure. *Rev. Mod. Phys.* **2000**, *72*, 621-654.
42. Kresse, G.; Furthmüller, J., Efficient Iterative Schemes for Ab Initio Total-Energy Calculations Using a Plane-Wave Basis Set. *Phys. Rev. B* **1996**, *54*, 11169-11186.
43. Kresse, G.; Furthmüller, J., Efficiency of Ab-Initio Total Energy Calculations for Metals and Semiconductors Using a Plane-Wave Basis Set. *Comp. Mater. Sci.* **1996**, *6*, 15-50.
44. Bahn, S. R.; Jacobsen, K. W., An Object-Oriented Scripting Interface to a Legacy Electronic Structure Code. *Comp. Sci. Eng.* **2002**, *4*, 56-66.
45. Blöchl, P. E., Projector Augmented-Wave Method. *Phys. Rev. B* **1994**, *50*, 17953-17979.

46. Kresse, G.; Joubert, D., From Ultrasoft Pseudopotentials to the Projector Augmented-Wave Method. *Phys. Rev. B* **1999**, *59*, 1758-1775.
47. Wellendorff, J.; Lundgaard, K. T.; Møgelhøj, A.; Petzold, V.; Landis, D. D.; Nørskov, J. K.; Bligaard, T.; Jacobsen, K. W., Density Functionals for Surface Science: Exchange-Correlation Model Development with Bayesian Error Estimation. *Phys. Rev. B* **2012**, *85*, 235149.
48. Dudarev, S. L.; Botton, G. A.; Savrasov, S. Y.; Humphreys, C. J.; Sutton, A. P., Electron-Energy-Loss Spectra and the Structural Stability of Nickel Oxide: An Lsda+U Study. *Phys. Rev. B* **1998**, *57*, 1505-1509.
49. Maurer, F., et al., Surface Noble Metal Concentration on Ceria as a Key Descriptor for Efficient Catalytic CO Oxidation. *ACS Catal.* **2022**, 2473-2486.
50. Monkhorst, H. J.; Pack, J. D., Special Points for Brillouin-Zone Integrations. *Phys. Rev. B* **1976**, *13*, 5188-5192.
51. Bordiga, S.; Groppo, E.; Agostini, G.; van Bokhoven, J. A.; Lamberti, C., Reactivity of Surface Species in Heterogeneous Catalysts Probed by in Situ X-Ray Absorption Techniques. *Chem. Rev.* **2013**, *113*, 1736-850.
52. Meunier, F. C., Relevance of Ir Spectroscopy of Adsorbed Co for the Characterization of Heterogeneous Catalysts Containing Isolated Atoms. *J. Phys. Chem. C* **2021**, *125*, 21810-21823.
53. Wöll, C., Structure and Chemical Properties of Oxide Nanoparticles Determined by Surface-Ligand Ir Spectroscopy. *ACS Catal.* **2020**, *10*, 168-176.
54. Lamberti, C.; Zecchina, A.; Groppo, E.; Bordiga, S., Probing the Surfaces of Heterogeneous Catalysts by in Situ Ir Spectroscopy. *Chem. Soc. Rev.* **2010**, *39*, 4951-5001.
55. Wang, C.; Gu, X.-K.; Yan, H.; Lin, Y.; Li, J.; Liu, D.; Li, W.-X.; Lu, J., Water-Mediated Mars–Van Krevelen Mechanism for Co Oxidation on Ceria-Supported Single-Atom Pt_1 Catalyst. *ACS Catal.* **2017**, *7*, 887-891.
56. Zhang, B.; Asakura, H.; Yan, N., Atomically Dispersed Rhodium on Self-Assembled Phosphotungstic Acid: Structural Features and Catalytic CO Oxidation Properties. *Ind. Eng. Chem. Res.* **2017**, *56*, 3578-3587.
57. Lu, Y., Wang, J.; Yu, L.; Kovarik, L.; Zhang, X.; Hoffman, A. S.; Gallo, A.; Bare, S. R.; Sokaras, D.; Kroll, T.; *et al.*, Identification of the Active Complex for CO Oxidation over Single-Atom Ir-on-$MgAl_2O_4$ Catalysts. *Nat. Catal.* **2019**, *2*, 149-156.
58. Hülsey, M. J.; Zhang, B.; Ma, Z.; Asakura, H.; Do, D. A.; Chen, W.; Tanaka, T.; Zhang, P.; Wu, Z.; Yan, N., In Situ Spectroscopy-Guided Engineering of Rhodium Single-Atom Catalysts for CO Oxidation. *Nat. Commun.* **2019**, *10*, 1330.
59. Muravev, V.; Spezzati, G.; Su, Y.-Q.; Parastaev, A.; Chiang, F.-K.; Longo, A.; Escudero, C.; Kosinov, N.; Hensen, E. J. M., Interface Dynamics of Pd–CeO_2 Single-Atom Catalysts During CO Oxidation. *Nat. Catal.* **2021**, *4*, 469-478.
60. Sarma, B. B.; Plessow, P. N.; Agostini, G.; Concepción, P.; Pfänder, N.; Kang, L.; Wang, F. R.; Studt, F.; Prieto, G., Metal-Specific Reactivity in Single-Atom Catalysts: CO Oxidation on 4d and 5d Transition Metals Atomically Dispersed on MgO. *J. Am. Chem. Soc.* **2020**, *142*, 14890-14902.
61. Chin, S. Y.; Williams, C. T.; Amiridis, M. D., FtIR Studies of CO Adsorption on Al_2O_3- and SiO_2-Supported Ru Catalysts. *J. Phys. Chem. B* **2006**, *110*, 871-882.
62. Li, J.; Liu, Z.; Cullen, D. A.; Hu, W.; Huang, J.; Yao, L.; Peng, Z.; Liao, P.; Wang, R., Distribution and Valence State of Ru Species on CeO_2 Supports: Support Shape Effect and Its Influence on CO Oxidation. *ACS Catal.* **2019**, *9*, 11088-11103.
63. Hafshejani, T. M.; Wang, W.; Heggemann, J.; Nefedov, A.; Heissler, S.; Wang, Y.; Rahe, P.; Thissen, P.; Wöll, C., CO Adsorption on the Calcite(10.4) Surface: A Combined Experimental and Theoretical Study. *Phys. Chem. Chem. Phys.* **2021**, *23*, 7696-7702.

64. Wang, Y.; Wöll, C., IR Spectroscopic Investigations of Chemical and Photochemical Reactions on Metal Oxides: Bridging the Materials Gap. *Chem. Soc. Rev.* **2017**, *46*, 1875-1932.
65. Lustemberg, P. G.; Plessow, P. N.; Wang, Y.; Yang, C.; Nefedov, A.; Studt, F.; Wöll, C.; Ganduglia-Pirovano, M. V., Vibrational Frequencies of Cerium-Oxide-Bound CO: A Challenge for Conventional DFT Methods. *Phys. Rev. Lett.* **2020**, *125*, 256101.
66. Sarangi, R.; Aboelella, N.; Fujisawa, K.; Tolman, W. B.; Hedman, B.; Hodgson, K. O.; Solomon, E. I., X-Ray Absorption Edge Spectroscopy and Computational Studies on $LCuO_2$ Species: Superoxide−Cu^{II} Versus Peroxide−Cu^{III} Bonding. *J. Am. Chem. Soc.* **2006**, *128*, 8286-8296.
67. Yang, C.; Garl, C. W., Infrared Studies of Carbon Monoxide Chemisorbed on Rhodium. *J. Phys. Chem.* **1957**, *61*, 1504-1512.
68. Matsubu, J. C.; Yang, V. N.; Christopher, P., Isolated Metal Active Site Concentration and Stability Control Catalytic CO_2 Reduction Selectivity. *J. Am. Chem. Soc.* **2015**, *137,* 3076-84.
69. Basini, L.; Marchionna, M.; Aragno, A., Drift and Mass Spectroscopic Studies on the Reactivity of Rhodium Clusters at the Surface of Polycrystalline Oxides. *J. Phys. Chem.* **1992**, *96*, 9431-9441.
70. Jbir, I.; Couble, J.; Khaddar-Zine, S.; Ksibi, Z.; Meunier, F.; Bianchi, D., Individual Heat of Adsorption of Adsorbed CO Species on Palladium and Pd–Sn Nanoparticles Supported on Al_2O_3 by Using Temperature-Programmed Adsorption Equilibrium Methods. *ACS Catal.* **2016**, *6*, 2545-2558.
71. Lu, J.; Serna, P.; Aydin, C.; Browning, N. D.; Gates, B. C., Supported Molecular Iridium Catalysts: Resolving Effects of Metal Nuclearity and Supports as Ligands. *J. Am. Chem. Soc.* **2011**, *133*, 16186-16195.
72. Debefve, L. M.; Hoffman, A. S.; Yeh, A. J.; Runnebaum, R. C.; Shulda, S.; Richards, R. M.; Arslan, I.; Gates, B. C., Iridium Atoms Bonded to Crystalline Powder MgO: Characterization by Imaging and Spectroscopy. *J. Phys. Chem. C* **2020**, *124*, 459-468.
73. Kottwitz, M., Li, Y.; Palomino, R. M.; Liu, Z.; Wang, G.; Wu, Q.; Huang, J.; Timoshenko, J.; Senanayake, S. D.; Balsubramanian, M.; *et al.*, Local Structure and Electronic State of Atomically Dispersed Pt Supported on Nanosized CeO_2. *ACS Catal.* **2019**, *9*, 8738-8748.
74. Aleksandrov, H. A.; Neyman, K. M.; Hadjiivanov, K. I.; Vayssilov, G. N., Can the State of Platinum Species Be Unambiguously Determined by the Stretching Frequency of an Adsorbed CO Probe Molecule? *Phys. Chem. Chem. Phys.* **2016**, *18*, 22108-22121.
75. Lu, Y., Zhou, S.; Kuo, C-T.; Kunwar, D.; Thompson, C.; Hoffman, A. S.; Boubnov, A.; Lin, S.; Datye, A. K.; Guo, H.; *et al.*, Unraveling the Intermediate Reaction Complexes and Critical Role of Support-Derived Oxygen Atoms in CO Oxidation on Single-Atom Pt/CeO_2. *ACS Catal.* **2021**, *11*, 8701-8715.
76. Meunier, F. C., On the Contamination with Nickel and Nickel Tetracarbonyl During Ft-IR Investigation of Catalysts under CO-Containing Gases. *J. Catal.* **2019**, *372*, 388.
77. Mudiyanselage, K.; Kim, H. Y.; Senanayake, S. D.; Baber, A. E.; Liu, P.; Stacchiola, D., Probing Adsorption Sites for CO on Ceria. *Phys. Chem. Chem. Phys.* **2013**, *15*, 15856-15862.
78. Binet, C.; Daturi, M.; Lavalley, J.-C., IR Study of Polycrystalline Ceria Properties in Oxidised and Reduced States. *Catal. Today* **1999**, *50*, 207-225.
79. Meunier, F. C., In Situ Formation of $Ni(CO)_4$ Contaminant During IR Analyses Using a Metal-Containing Reaction Cell. *Catal. Sci. Tech.* **2022**, *12*, 7433-7438.
80. Yao, Y.; Chen, L.; Mao, X.; Yang, Y.; Chen, J.; Zhou, L., In Situ PM-IRRAS Study of CO Adsorption on Au Surfaces: Solving the Puzzle. *J. Phys. Chem. C* **2021**, *125*, 8606-8619.

81. Spezzati, G.; Su, Y.; Hofmann, J. P.; Benavidez, A. D.; DeLaRiva, A. T.; McCabe, J.; Datye, A. K.; Hensen, E. J. M., Atomically Dispersed Pd–O Species on CeO_2(111) as Highly Active Sites for Low-Temperature CO Oxidation. *ACS Catal.* **2017**, *7*, 6887-6891.
82. Mizushima, T.; Tohji, K.; Udagawa, Y.; Ueno, A., Exafs Study of the Carbon Monoxide Adsorption-Induced Morphology Change in Ruthenium Clusters Supported on Alumina. *J. Phys. Chem.* **1990**, *94*, 4980-4985.
83. Dictor, R.; Roberts, S., Morphological Changes of Rhodium on Alumina as Observed by Using Fourier Transform Infrared Spectroscopy. *J. Phys. Chem.* **1989**, *93*, 2526-2532.
84. Solymosi, F.; Novak, E.; Molnar, A., Infrared Spectroscopic Study on Carbon Monoxide-Induced Structural Changes of Iridium on an Alumina Support. *J. Phys. Chem.* **1990**, *94*, 7250-7255.
85. Ding, K.; Gulec, A.; Johnson Alexis, M.; Schweitzer Neil, M.; Stucky Galen, D.; Marks Laurence, D.; Stair Peter, C., Identification of Active Sites in CO Oxidation and Water-Gas Shift over Supported Pt Catalysts. *Science* **2015**, *350*, 189-192.
86. Hulva, J.; Meier, M.; Bliem, R.; Jakub, Z.; Kraushofer, F.; Schmid, M.; Diebold, U.; Franchini, C.; Parkinson Gareth, S., Unraveling CO Adsorption on Model Single-Atom Catalysts. *Science* **2021**, *371*, 375-379.
87. Feng, K.; Zhang, H.; Gao, J.; Xu, J.; Dong, Y.; Kang, Z.; Zhong, J., Single Atoms or Not? The Limitation of Exafs. *Appl. Phys. Lett.* **2020**, *116*, 191903.

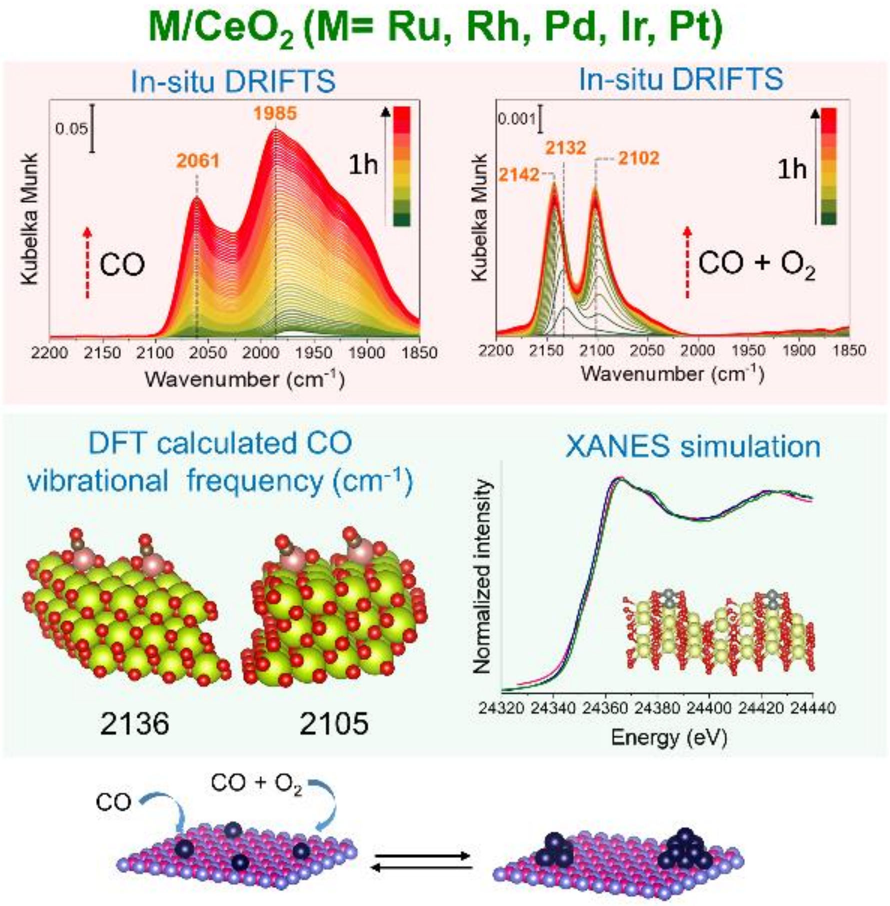

Table of content (TOC)